Evaluating Common-View Time Transfer Using a Low-Cost Dual-Frequency GNSS Receiver

Aidan A. Montare, Andrew N. Novick, Jeff A. Sherman, *National Institute of Standards and Technology*

Biographies

Aidan Montare is an electronics engineer at NIST's Time and Frequency Division in Boulder, Colorado. Aidan works to improve and develop NIST's remote calibration services and researches new time transfer systems. Aidan is also a member of the Ham Radio Citizen Science Investigation (HamSCI), where she works to make NIST's time and frequency services useful to scientists studying the upper atmospheric and space physics. She is a graduate of Case Western Reserve University in Cleveland, Ohio, and an alumni of the Case Amateur Radio Club W8EDU.

Andrew Novick is an electrical engineer in the Time and Frequency Division at NIST. He manages and maintains the remote clock and oscillator calibration services and other monitoring and research projects. Novick also developed and maintains the national web clock, *www.time.gov*, and he is the division's Quality Manager.

Jeff Sherman is a physicist in the Time and Frequency Division at NIST and leads the Time Realization and Distribution group. This group is responsible for continuous operation, distribution, and improvement of an ensemble of atomic clocks which produce UTC(NIST), NIST's live realization of Coordinated Universal Time. Group activities also include measurement of primary atomic frequency standards based on cesium and optical frequency standards.

Abstract

Common-view time transfer can be performed using either single (L1) or dual (L1/L2 or L1/L5) frequency global navigation satellite system (GNSS) signals. Using dual-frequency receivers for common-view has advantages but has historically been of significantly higher cost. In this work we evaluate the performance of a common-view time transfer system based on a new low-cost dual-frequency GNSS receiver. The receiver features built-in time-tagging capabilities, reducing overall system cost by eliminating separate time interval counter (TIC) hardware. We compare this system to an existing common-view system that uses an external TIC and a single-frequency receiver.

Based on prior work, we expect short-baseline common-clock measurements to have a time deviation evaluated at 1 day of less than 1 ns and that the increased short-term noise of integrated time-tagging functionality versus a dedicated TIC will become inconsequential at averaging intervals of 5 min or more.

We compare the systems in terms of both position determination and time transfer performance, including diurnal variations. We also compare integrated versus separate TIC functionalities. We evaluate time transfer performance in a variety of scenarios, including common-antenna common-clock, short baseline common-clock, and longer baselines with different clocks. In these experiments, we aim to demonstrate that modern systems can achieve equivalent performance at lower cost, providing a robust foundation for future measurements.

1 INTRODUCTION

Common-view time transfer is an established technique for real-time clock comparisons. In this method, two or more stations simultaneously observe wavefronts from a source and measure their arrival time; differences between any two stations can be found via subtraction of the measurements (Allan & Weiss, 1980; Levine, 2008).

GNSS receivers that track a single GNSS frequency have been, and remain, the lowest cost option for performing common-view but, recently, inexpensive dual-frequency receivers have come to market. Dual-frequency receivers offer notable advantages, in particular, their ability to minimize ionospheric effects via measurement rather than modeling (Chen et al., 2017).

The ionospheric delay of GNSS signals is frequency dependent. Dual-frequency receivers use observations from two frequencies to measure and cancel the ionospheric delay to first order. The resultant measurement is called the "ionosphere-free combination" and follows the following equation:

$$R_{iono-free} = \frac{{f_1}^2 R_1 - {f_2}^2 R_2}{{f_1}^2 - {f_2}^2}$$

where R_1 and R_2 are the raw observables from the receiver's code measurement from each frequency, and f_1 and f_2 are the carrier frequencies of each signal (*IS-GPS-200N*, 2022; Subirana et al., 2011). Dual-frequency receivers apply this correction and report corrected measurements for each satellite.

In this report, we evaluate the performance of such a dual-frequency receiver, the u-blox ZED-F9T timing receiver[1], in various aspects that affect the performance of a time transfer system. This receiver also features internal time-tagging of input signals, which has the potential to further reduce system costs by eliminating the external TIC that would typically be used.

We evaluate the performance of the receiver in three areas: position determination, time-tagging, and time transfer. Of note, we compare time transfer using a prototype system based on this receiver with time transfer using a well-established common-view service, the NIST Time Measurement and Analysis Service (TMAS) (Lombardi & Novick, 2006; Novick, 2023).

2 POSITION DETERMINATION

Accurately determining antenna position is important for a common-view system, as errors in position translate into timing errors. Due to the geometry of the problem, vertical (height) positioning errors are the most detrimental to timing performance (Lombardi, 2016). Since each meter of vertical error corresponds to up to 3.3 ns of timing error, we desired a height accuracy of 30 cm or less for our system.

The receiver under study features a built-in configurable survey mode that produces a weighted-average position, after which the receiver fixes its position estimate and uses GNSS signals for a timing-only solution; it was this method that we evaluated.

Using a single-frequency receiver with a 24-hour survey period, height determination is generally accurate within 10 m, but is sometimes greater than 15 m, leading to a timing error that approaches 50 ns (Lombardi, 2016; Lombardi et al., 2014).

2.1 Methods

To evaluate the position determination of the receiver, we developed software to run repeated surveys of various durations and record the results. Both raw readings and the receiver's reported final position were collected for analysis.

The antenna was mounted on a rooftop pole whose position had already been determined via a 24-hour survey with a geodetic receiver utilizing an L-band satellite augmentation service with a stated accuracy of height determination of 20 cm. As an additional point of comparison, raw measurements from the receiver were used to produce Receiver Independent Exchange Format (RINEX) files (via the *convbin* tool from the *rtklib* package (Takasu, 2013)), which were submitted to Natural Resources Canada's (NRCan) online precise point positioning (PPP) service (Canadian Geodetic Survey, 2023).

The PPP technique provides accurate positioning by combining a receiver's raw measurements with data, i.e. satellite clock and orbit information, from global networks of monitoring stations. PPP solutions can reach centimeter-level precision at the cost of additional complexity and the additional delays in processing (Elsheikh et al., 2023; Leandro et al., 2011). For example, the highest-accuracy satellite orbit and clock data from the International GNSS Service (IGS) are available with a latency of 12 days to 18 days (Choy et al., 2017). Since common-view timing measurements are usually made with fixed-position antennas, a one-time PPP measurement at a site to achieve height accuracy < 20 cm is worth the processing delay. For the antenna pole used in these tests, the geodetic survey results only differed from the PPP result by 2.4 cm.

2.2 Results

Figure 1 shows how the receiver's height estimate evolves over the duration of a 24-hour survey. In the multiple cold-start surveys performed, the receiver reliably gets within 2 m of the PPP solution after about 6 h, and within 1 m after 18 h. The

---

[1] *Commercial equipment is identified for informational purposes only. Such identification does not imply recommendation or endorsement by the National Institute of Standards and Technology, nor does it imply that the equipment is necessarily the best available for purpose.*

final results of these surveys have a total dispersion of about 0.5 m, suggesting reasonable repeatability of the survey process. The maximum excursions in the first few minutes of surveying were up to 18 m (outside of the range shown on the figure). The final results are biased high relative to the PPP solution, the cause of which has not yet been identified and thus do not meet the ±30 cm accuracy goal stated earlier. However, the dual-frequency receiver is clearly superior to a single frequency receiver in height determination. For users desiring greater position accuracy, a PPP solution can be computed after the fact.

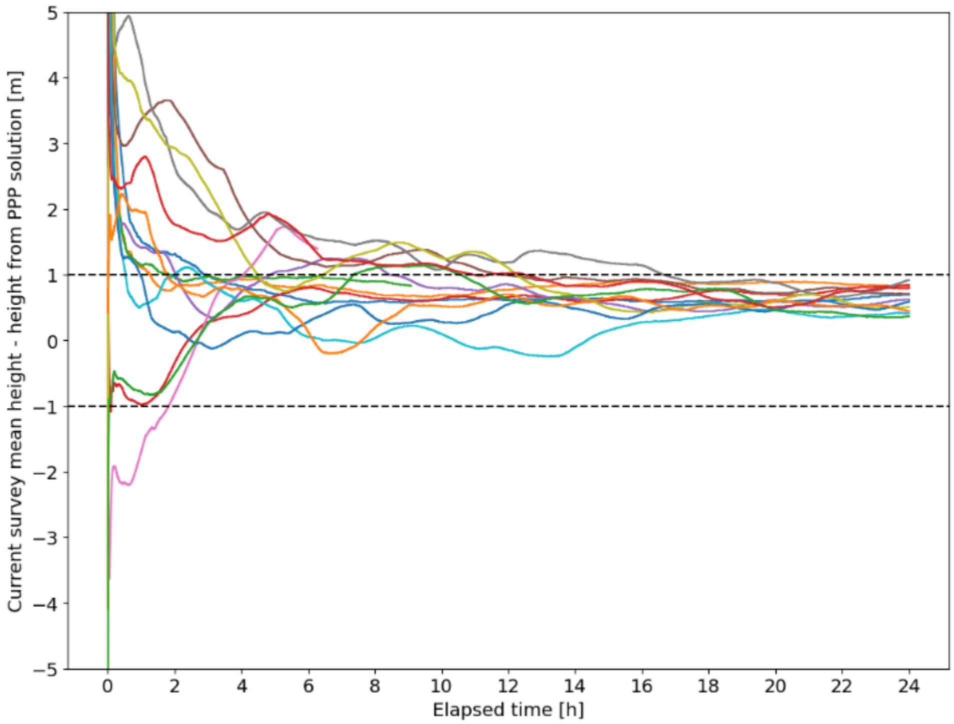

FIGURE 1 Mean survey height (relative to the PPP solution) as a function of survey time for n = 14 independent 24-hour surveys. Dashed lines indicate ±1 m around the PPP solution.

3 TIME-TAGGING

The selected receiver features internal time-tagging of pulse inputs with an advertised resolution of 8 ns (*ZED-F9T-00B Data Sheet*, 2022). When a pulse is provided on an interrupt pin, the time of the pulse in the receiver timebase is reported at the next epoch. It is perhaps of note that the receiver documentation explicitly describes the use of this functionality for common-view time transfer (*ZED-F9T Integration Manual*, 2022). In common-view time transfer, a separate TIC is typically used to measure the receiver's on-time pulse versus the input signal (Lombardi et al., 2001). By providing potentially equivalent functionality within the receiver, the external TIC could be eliminated, reducing system costs. Typical TICs used in common-view measurements have a resolution in the tens of picoseconds, much better than the 8-ns range of the internal time-tagging.

3.1 Methods

To evaluate the performance of the receiver's internal time-tagging functionality, we conducted a common-clock common-view experiment and analyzed the data in two different ways: using the receiver's internal time-tagging and using standalone laboratory TICs with a resolution of 50 ps measuring the 1 pulse per second (PPS) output of the receivers. A block diagram of the experimental setup is shown in Figure 2.

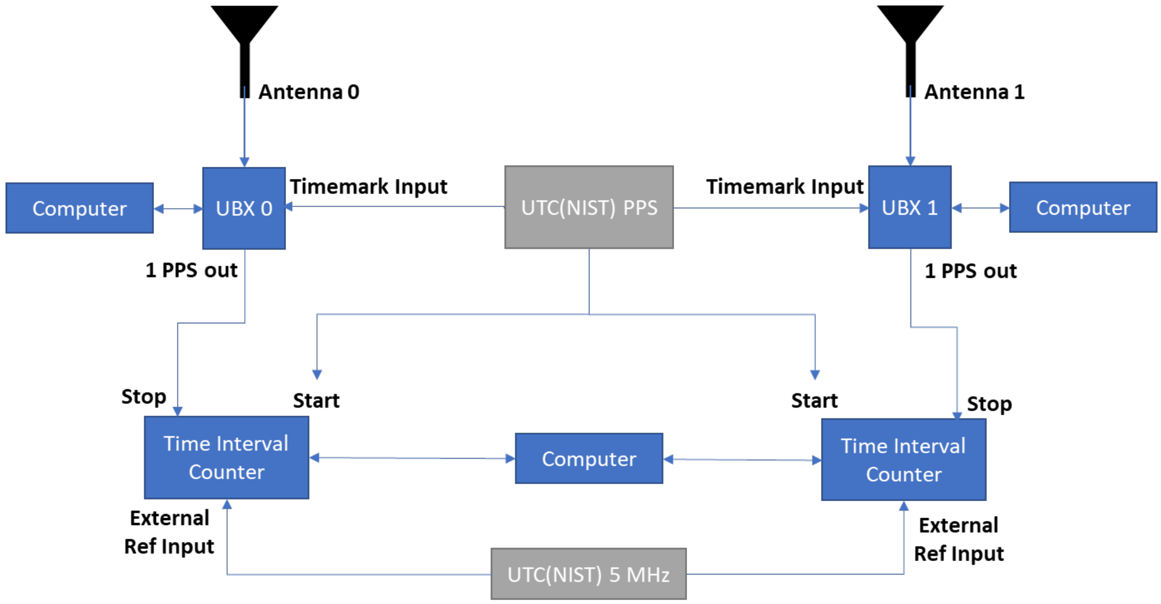

FIGURE 2 Experimental setup for comparing receiver time-tagging with external counters with a short baseline (less than 15 m). Both receiver and counter data were collected so that a common-view difference could be computed either using the receiver time-tagging or TIC results.

3.2 Results

Common-view averages between the two receivers over a period of about 8 d are shown in Figure 3. As expected, the receiver time-tagging exhibits a much larger range of values due to its lower precision. However, the Time Deviation (TDEV) plot shows that this short-term noise benefits from averaging. After less than a minute of averaging, the TDEV of the receiver time-tagging method is below a nanosecond. For all subsequent averaging intervals neither method has a TDEV greater than a nanosecond and the results appear to converge at about 2000 s. At 300 s to 600 s (5 min to 10 min), receiver time-tagging, while still noisier than the external TIC, is below the noise we would typically expect for common-view. This suggests that internal time-tagging is an appropriate choice for real-time systems that average for 5 min or more.

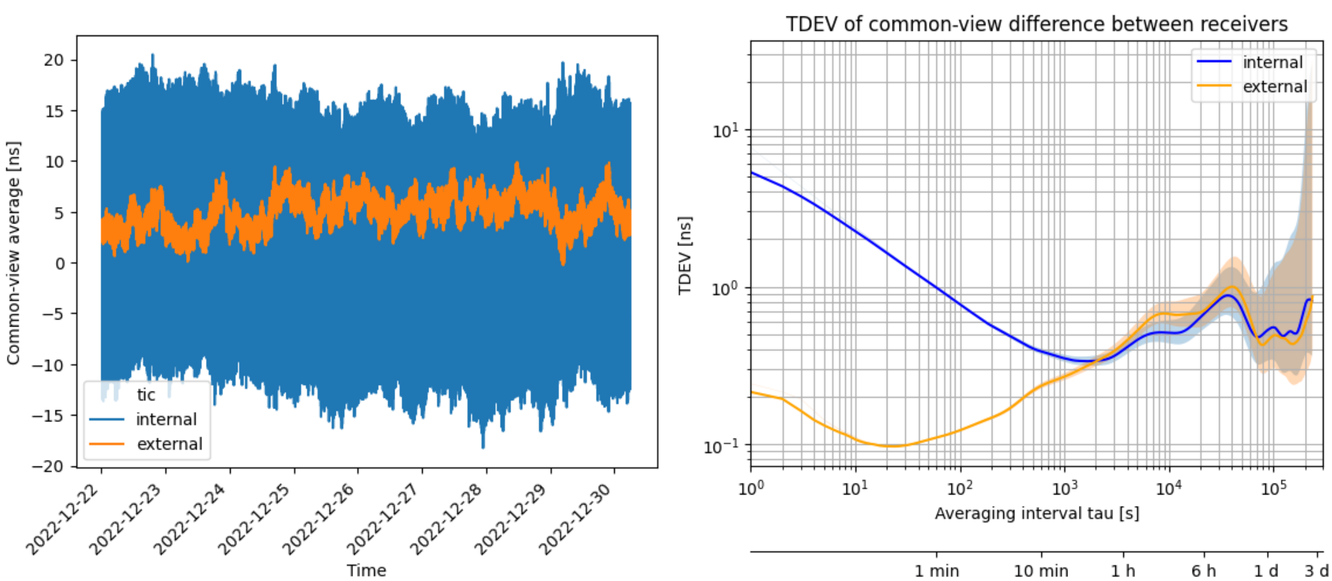

FIGURE 3 Common-view average between u-blox receivers measuring a common clock with internal (receiver built-in time-tagging) and external time interval counters, as (a) time series, (b) TDEV.

4 TIME TRANSFER

We evaluated time transfer performance over links of 3 different lengths: a near-zero baseline, a 78-km baseline, and an over-5000-km baseline. The near-zero baseline experiment measured a common clock to establish a lower floor of performance. The 78-km baseline experiment compared the UTC(NIST) time scale in Boulder, CO with an independent time scale at NIST radio station WWV in Ft. Collins, CO. The 5000-km baseline experiment compared UTC(NIST) in Boulder with a free-running cesium beam clock at NIST radio station WWVH in Kauai, Hawaii. The remote stations are summarized in the table. The local station in all experiments was in Boulder, CO and measuring the UTC(NIST) timescale.

TABLE 1

Common-view Experiments Performed

	Remote Location	Remote Clock	Baseline
Near-zero	Boulder, CO	UTC(NIST)	2.4 m
Short-medium	Ft. Collins, CO	Secondary UTC(NIST) time scale	78 km
Very long	Kauai, HI	Free-running cesium clock	5314 km

4.1 Methods

At all three locations, a single-frequency common-view unit (as part of the TMAS network) was either already available or was installed to provide a comparison for the dual-frequency prototype system.

The prototype system reported measurements per satellite over 10 min averaging periods using the same text format created for the TMAS system for ease of comparison and analysis. Measurements from both existing and prototype systems were uploaded every 10 min to a cloud server to allow access to the data and computation of common-view differences between any pair of systems. Based on results like those in Section 3, the prototype system used the receiver's internal time-tagging, while the existing system uses a separate TIC.

The prototype system was calibrated by comparing 5 d of data in common-view with a reference system for the existing common-view service and taking the average offset as the correction value.

4.2 Results

A so-called "one-way" time transfer plot is made by calculating the average of the differences between observed GNSS satellites and the clock being measured at a chosen averaging interval. A plot of the one-way averages helps visualize the performance of a single measurement device, though the common-view performance will be better by the degree to which common-mode effects cancel between sites when the measurements are differenced.

Figure 4 shows a one-way plot of 10-min averages over a 23-day period from both an existing single-frequency system (blue) and the dual-frequency prototype system (orange). The figure highlights the decreased diurnal variations present in the dual-frequency data, presumed to be due to greater cancelation of ionospheric effects. As a result, the range of the dual-frequency data is much smaller compared to the single-frequency data.

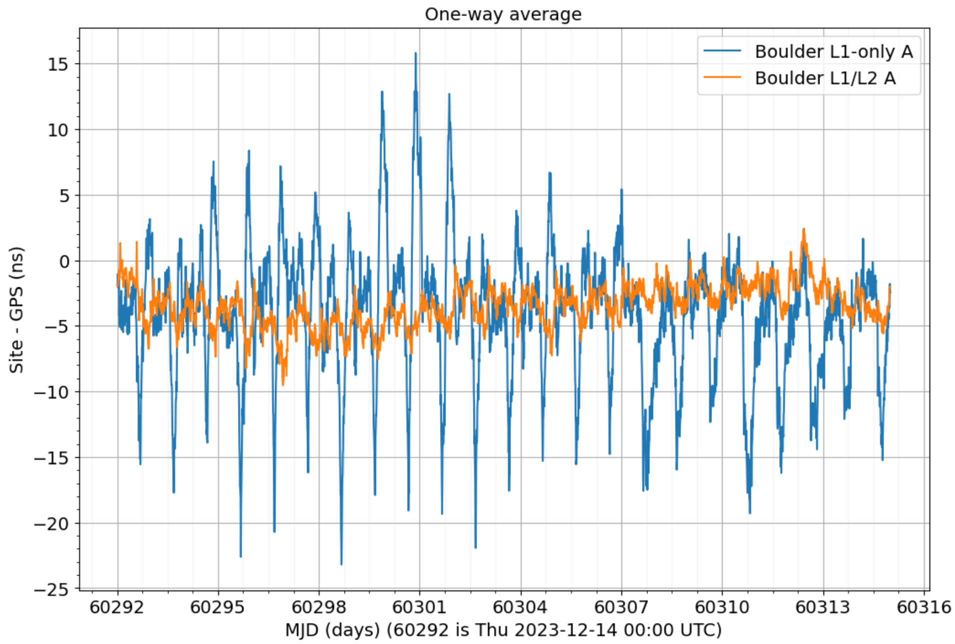

FIGURE 4 One-way GPS plot over a 23-day period from a single-frequency receiver (blue) and a dual-frequency receiver (orange) at the same location (2.4 m baseline).

Figure 5 shows the results of common-view measurement over the near-zero baseline as both a time series and a TDEV plot. Both single and dual-frequency common-view measurements show marked improvement over their one-way counterparts. Measurements from the dual-frequency system again have a lower range compared to the single-frequency system. Note that the range and diurnal variations are also reduced for the dual-frequency receivers. While the effects due to the ionosphere are the same on a relatively short baseline, the improvements with the dual-frequency common-view comes from better cancellation. The dual-frequency measurements show a lower TDEV statistic at all averaging intervals. After over a week, single and dual-frequency results appear to begin converging.

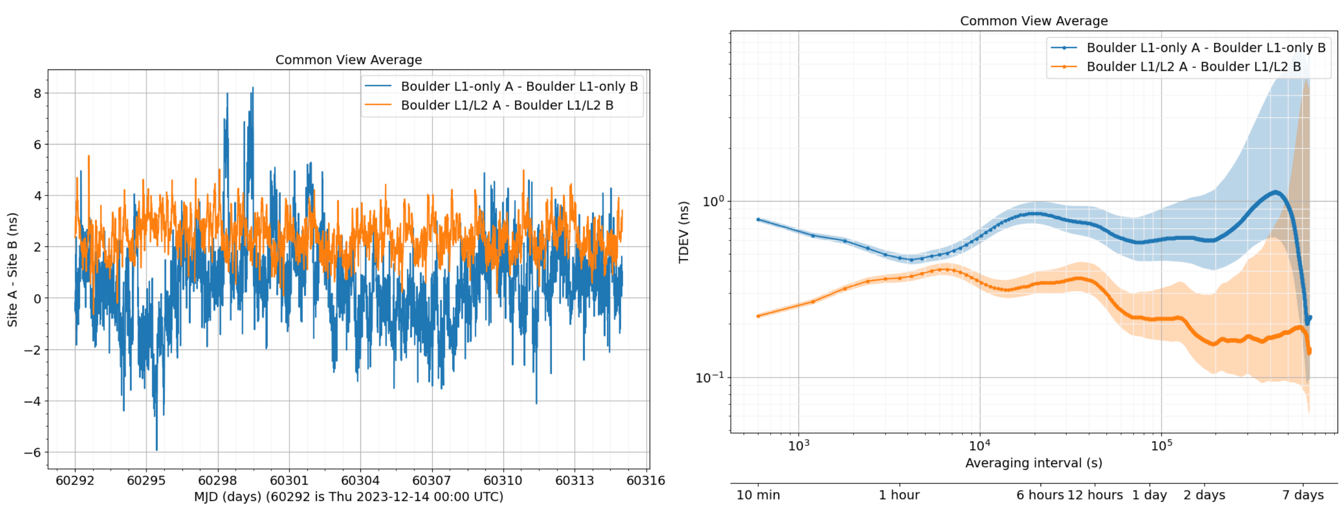

FIGURE 5 Common-view measurements of a common clock over a near-zero baseline as (a) time series and (b) TDEV statistic. Measurements shown in blue are between existing single-frequency systems; those shown in orange are between dual-frequency systems.

Figure 6 shows the results of the 78-km-baseline experiment. The reference at the WWV site had a frequency offset of 3.7×10^{-13} during this period, as shown by both measurements. However, the dual-frequency system once again displays a smaller range. The two lines are separated by several nanoseconds, It is possible that the single-frequency measurement system, which has been at the remote for many years, needs to be re-calibrated for delays. The TDEV plot highlights that the dual-frequency system offers as much as a factor-of-two improvement over averaging intervals of less than 1 day. The TDEV plot does not continue to average down and reaches about 1 ns due to the performance of the remote time scale. The single- and dual-frequency common-view measurements begin to converge sooner in this experiment, at about 2 d to 3 d.

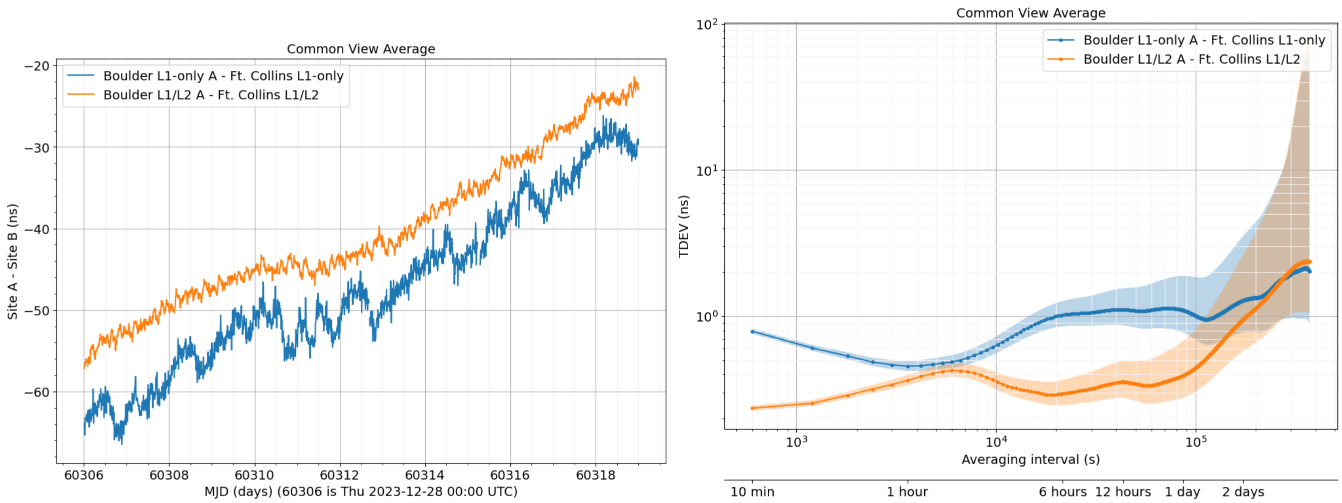

FIGURE 6 Common-view measurements over a 78-km baseline between Boulder (UTC(NIST) time scale) and Ft. Collins, CO (an independent secondary time scale with a frequency offset of 3.7×10^{-13} during this interval). Measurements shown in blue are between two single-frequency systems; those shown in orange are between two dual-frequency systems.

Figure 7 shows the results of the 5314-km-baseline experiment. Over such a large baseline, the single-frequency common-view difference has a range of up to roughly 50 ns over a single day. The dual-frequency difference has a much lower range of about 10 ns or less over a day. The TDEV shows as much as a factor-of-nine improvement over the single-frequency system at averaging intervals less than a day. The TDEV of the dual-frequency data reaches above 1 ns at less than six hours (partially due to the clock being measured). Single- and dual-frequency measurements again converge after two days to three days of averaging, slightly sooner than the previous experiment.

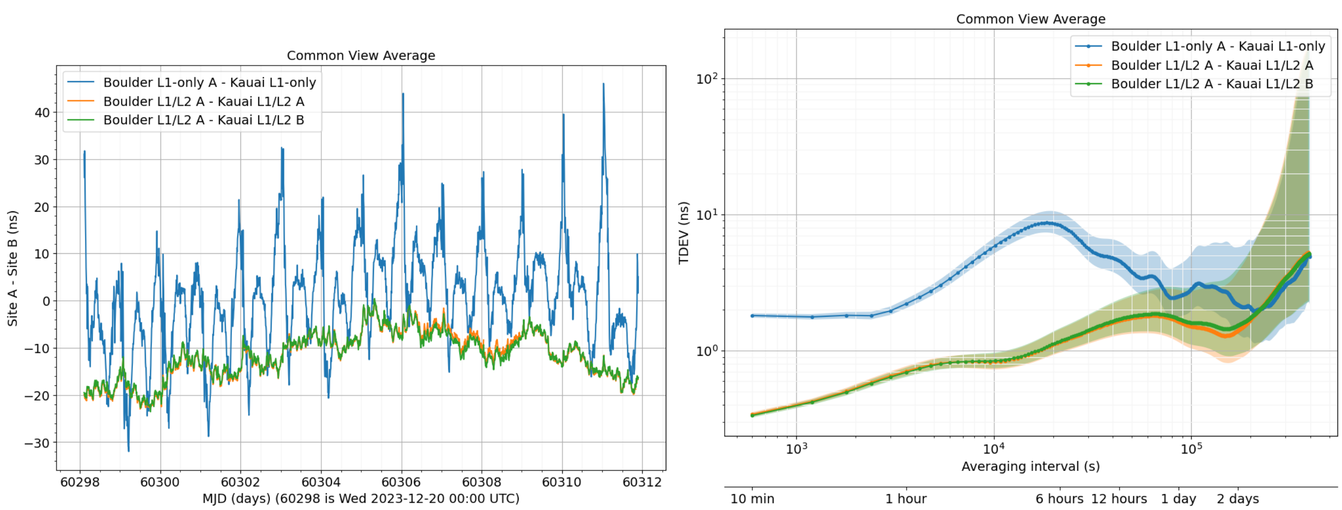

FIGURE 5 Common-view measurements over a 5314 km baseline between Boulder, CO (UTC(NIST) timescale) and Kauai, HI (free-running commercial cesium beam clock). Measurements shown in blue are between the two single-frequency systems. Two identical dual-frequency systems were present at Kauai measuring the same signal; their common-view differences are shown in orange and green.

5 CONCLUSIONS

After evaluating the use of the dual-frequency receiver with internal time-tagging, we believe it has good potential for use in time transfer applications. The receiver features improved positioning accuracy over a single frequency receiver and has the option to create data formatted for post-processing if greater accuracy is desired. The built-in time-tagging functionality adds short term noise, which averages out relatively quickly, and the TDEV is equivalent to a high-resolution TIC thereafter, allowing for reduced system cost. The one-way and common-view time transfer performance of the dual-frequency receiver shows the expected improvement over a single-frequency receiver.

In future work, we hope to expand on this progress by evaluating the dual-frequency time-tagging receiver in additional ways. For instance, the receiver we tested can utilize signals from several GNSS constellations, although we only used it with GPS data. Therefore, a study of one-way and common-view time transfer using intercomparisons of the different constellations could be performed. Also, demonstrating the use of this receiver in common-view disciplined clock systems would be highly valuable for future services.

ACKNOWLEDGMENTS

The authors would like to thank their colleagues at NIST radio stations WWV (Bill Yates, Jim Spicer, Glenn Nelson, Matt Deutch) and WWVH (Chris Fujita, Steve Johnston) for their support in these experiments. We would also like to thank Mike Lombardi for his development of the NIST TMAS service and for his mentorship.

This work was supported by the National Institute of Standards and Technology Physical Measurement Laboratory, an agency of the U.S. government, and is not subject to U.S. copyright.

REFERENCES

Allan, D. W., & Weiss, M. A. (1980). Accurate Time and Frequency Transfer During Common-View of a GPS Satellite. *34th Annual Symposium on Frequency Control*, 334–346. https://doi.org/10.1109/FREQ.1980.200424

Canadian Geodetic Survey. (2023, January 9). *Precise Point Positioning*. https://webapp.csrs-scrs.nrcan-rncan.gc.ca/geod/tools-outils/ppp.php?locale=en

Chen, J., Huang, L., Liu, L., Wu, P., & Qin, X. (2017). Applicability analysis of VTEC derived from the sophisticated Klobuchar model in China. *ISPRS International Journal of Geo-Information*, *6*(3), 75.

Choy, S., Bisnath, S., & Rizos, C. (2017). Uncovering common misconceptions in GNSS Precise Point Positioning and its future prospect. *GPS Solutions*, *21*(1), 13–22. https://doi.org/10.1007/s10291-016-0545-x

Elsheikh, M., Iqbal, U., Noureldin, A., & Korenberg, M. (2023). The Implementation of Precise Point Positioning (PPP): A Comprehensive Review. *Sensors*, *23*(21), Article 21. https://doi.org/10.3390/s23218874

Leandro, R. F., Santos, M. C., & Langley, R. B. (2011). Analyzing GNSS data in precise point positioning software. *GPS Solutions*, *15*(1), 1–13. https://doi.org/10.1007/s10291-010-0173-9

Levine, J. (2008). A review of time and frequency transfer methods. *Metrologia*, *45*(6), S162.

Lombardi, M. A. (2016). Evaluating the Frequency and Time Uncertainty of GPS Disciplined Oscillators and Clocks. *NCSLI Measure*, *11*(3–4), 30–44. https://doi.org/10.1080/19315775.2017.1316696

Lombardi, M. A., Nelson, L. M., Novick, A. N., & Zhang, V. S. (2001). Time and Frequency Measurements Using the Global Positioning System (GPS). *Proc. 2001 Meas. Sci. Conf.* https://tf.nist.gov/general/pdf/1417.pdf

Lombardi, M. A., & Novick, A. N. (2006). Remote Time Calibrations via the NIST Time Measurement and Analysis Service. *NCSLI Measure*, *1*(4), 50–59. https://doi.org/10.1080/19315775.2006.11721348

Lombardi, M. A., Novick, A. N., & Zhang, V. S. (2014). A Low-Cost Time Transfer Receiver for Contributions to Coordinated Universal Time. *Journal of Research of the National Institute of Standards and Technology*, *119*, 583–601. https://doi.org/10.6028/jres.119.024

NAVSTAR GPS Space Segment/Navigation User Segment Interfaces. (2022). https://www.gps.gov/technical/icwg/IS-GPS-200N.pdf

Novick, A. (2023, April 28). *Time Measurement and Analysis Service (TMAS)*. NIST. https://www.nist.gov/programs-projects/time-measurement-and-analysis-service-tmas

Subirana, J. S., Zornoza, J. M. J., & Hernández-Pajares, M. (2011). *Ionosphere-free Combination for Dual Frequency Receivers*. ESA Navipedia. https://gssc.esa.int/navipedia/index.php/Ionosphere-free_Combination_for_Dual_Frequency_Receivers

Takasu, T. (2013). *RTKLIB: An Open Source Program Package for GNSS Positioning*. https://www.rtklib.com/

ZED-F9T Integration manual. (2022). u-blox AG. https://content.u-blox.com/sites/default/files/ZED-F9T_IntegrationManual_UBX-21040375.pdf

ZED-F9T-00B Data Sheet. (2022). u-blox AG. https://content.u-blox.com/sites/default/files/ZED-F9T-00B_DataSheet_UBX-18053713.pdf